Advances in Nanochemistry

Article

Mass production of aluminium and aluminum oxide nanoparticles by electrical explosion of wire

Maryam Darvishpour [1], Davoud Yazdani [2], Mostafa Faizi [2], Mohammad Joshghani *[1,2]

Received 14th June 2019,
Accepted 11th July 2019,
DOI: 10.22126/anc.2019.4147.1014

[1] Department of Inorganic Chemistry, Faculty of Chemistry, Razi University, Kermanshah, 67149, Iran
[2] Department of Nanochemistry, Faculty of Chemistry, Razi University, Kermanshah, 67149, Iran

Abstract

Aluminum nanoparticles (AlNPs) and aluminum oxide (AlONPs) nanoparticles were selectively produced in large quantities by the electrical explosion of wire (EEW) process in different conditions. Transmission electron microscopy (TEM), laser particle size analyzing, X-ray diffraction (XRD), and Fourier-transform infrared (FT-IR) spectroscopy were carried out to characterize the purity, morphology, particle and crystallite size of the nanoparticles. The effects of wire diameter, feed rate, electrode distance, pulse time, voltage, carrier gas pressure, and fan pressure in the exploding wire chamber on the particle size were analyzed by a preliminary Taguchi design of experiment. The results show that the wire diameter, feed rate, pulse time, voltage, and electrode distance are the main five factors. An ultimate response surface methodology (RSM) design showed the particle size increases with decreasing voltage and increasing other factors.

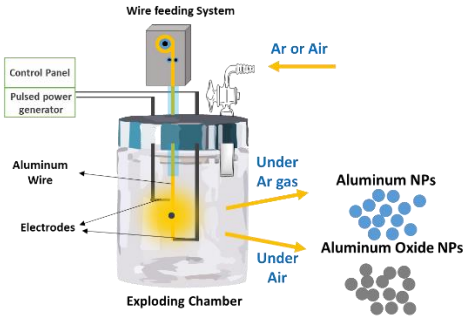

Keywords: *Electrical explosion of wire, Aluminum nanoparticles, Alumina nanoparticles, Design of experiments.*

Introduction

Aluminum nanoparticles (AlNPs) and alumina (AlONPs) nanoparticles have recently been attracted much attention because of their unique properties and have widely been studied in various fields, such as electronics devices and catalysis.[1-7] AlNPs are the most common ingredients for explosives and the most reactive metals due to their high heat of oxidation into the corresponding oxides, and their low cost.[6-9] AlONPs are suitable for preparing special ceramics with improved hardness and wear resistance as well as in membranes and catalyst preparation.[10-13]

The most important problem on the way toward wide applications of AlNPs and AlONPs is the dependence of their properties to the production conditions.[14] There are a wide variety of chemical and physical methods for production of AlNPs and AlONPs.[15-20] Most of these methods require costly precursors, templates, and harsh preparation conditions.

The electrical explosion of wire (EEW) which is basically a physical vapor deposition technique has been used for the production of nanopowders due to several advantages such as: (a) ability to produce nanopowders with high purity, (b) high energy efficiency, and (c) feasibility to be used for mass production.[21] This technique uses of both top-down and bottom-up approaches. The top-down process when the solid wire is disintegrated into vapor by the Joule heating effect and produce a supersaturated vapor. The bottom-up process during which nanoparticles are formed through the nucleation and subsequent growth of nuclei from the supersaturated vapor.[7] Several investigations have been carried out to determine the effect of various experimental factors on the characteristics of powder produced from the EEW. Some of these factors are: (i) ambient gas species and pressure,[22,23] (ii) energy deposited into the wire,[24-26] and (iii) initial crystalline structure of wire.[27]

Many papers have been published on different aspects of this method.[7,28-31] However, literatures on optimization of production protocol of EEW are scanty and still need to be investigated. Therefore, the objective of this study was optimization of mass production of AlNPs and AlONPs based on EEW by using design of experiments methods and prediction of the best preparation condition to produce nanoparticles having specific particle size.[32]

Experimental

General

X-ray diffraction (XRD) patterns were recorded on an Inel French, EQUINOX 3000 model X-ray diffractometer with Cu K_α radiation (λ= 1.5406, 30 kV, 20 mA). Transmission electron microscopy (TEM) were performed using a Jeol JEM-2100 transmission electron microscope with an accelerating voltage of 200 kV. The size distribution and zeta potential of the samples were obtained using a laser particle size analyzer (HPPS5001, Malvern, UK). Fourier transform infrared (FT-IR) spectra were recorded as KBr pellets using a Shimadzu 470 FT-IR spectrophotometer. Design of experiment (DOE) software Version 7.0.0 was used to investigate the statistical analysis of preparation of AlNPs by EEW.

Typical procedure for the synthesis of nanoparticles by EEW

The EEW experiments were carried out using a designed apparatus for mass production of nanoparticles.[28] The apparatus consists of a

Corresponding author:
Mohammad Joshaghani, Email: mioshaghani@razi.ac.ir

wire feeding system which continuously conducts wire into the EEW chamber with a defined rate. The aluminum wire acts as the upper electrode while a fixed aluminum plate at the bottom of explosion chamber acts as the lower electrode. The lower electrode was connected to a direct current power source. The voltage and the distance between electrodes were two of investigated operational factors. After each explosion the high voltage source was concurrently recharged and the feeding system kept advancing the wire, and the process was repeated again. In each experiment, the chamber was evacuated to 0.1 Pa pressure then the chamber was purged by argon three times.

On beginning, the current density is passed through the wire and the temperature of the wire rises by joule heating. The wire undergoes physical changes such as melting, boiling and vaporization. Some of surface evaporation from the wire takes place before the wire melts completely. On decreasing the thickness of wire, the current density passed through the wire is decreased significantly but the surface evaporation leads to formation of plasma of the wire materials which increases the current to some extent. As the wire materials completely melt, the current through the wire become negligible and when the concentration of the vapor reaches to a particular value, an arc discharge occurs. At this stage, a column of ionized plasma is formed. Subsequently, the plasma begins to expand due to the enormous difference in the temperature and pressure of the plasma and the ambient gas. The expanded plasma particles are rapidly cooled down during the expansion and a supersaturated vapor is formed which undergoes a homogeneous nucleation of nanoparticles.[7,30-36] The nanoparticles were collected and subjected to further studies.

Results and discussion

Experimental design and mathematical model

In order to obtain a mathematical model for prediction of a real system containing a number of factors, careful planning of experiments should be done.[37,38] Design of experiments is a statistical approach for modeling of an experimental response y by considering the most important effective factors $x_1, x_2, \ldots, x_k$ as (equation 1):

$$y = f(x_1, x_2, \ldots, x_k) \quad (1)$$

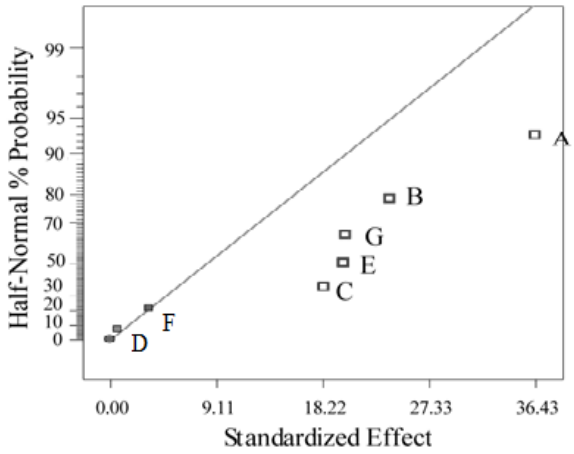

Figure 1. *Half–Normal % probability vs. standardized effect plot for each factor based on preliminary design by Taguchi method (D and F factors that are on the line have negligible effect on the response).*

Designing methods are often viewed as a three-step process: i) system design, ii) factor design, iii) tolerance design. System design involves determining which factors may have the greatest influence on the response. The selected factors are the factors of the design, and their magnitude are referred as levels. The outputs of system which are recorded and analyzed are the responses. Statistical analyses are used to find the optimum levels for each factor. The Taguchi method is one of the easiest designing methods to study a large number of factors with a small number of experiments. The Taguchi method has developed into an established approach for analyzing interaction effects when ranking and screening various controllable factors. Moreover, this method is applicable to solving a variety of problems involving continuous, discrete, and qualitative design variables. The Taguchi method uses an orthogonal array designated by L_n, where n is the number of rows or individual experiments.[39,40] In this work a preliminary design was performed with Taguchi model to eliminate the less important factors. The remaining important factors were studied comprehensively by response surface method (RSM) method (equation (2)).[41]

$$Y = \beta_0 + \beta_i X_i + \beta_j X_j + \beta_{ii} X_i^2 + \beta_{jj} X_j^2 + \beta_{ij} X_i X_j + \cdots \quad (2)$$

Where, *i* and *j* are the linear and quadratic indexes, respectively, and β is the regression coefficient. X_i and X_j are the studied independent factors. β_0 is the interception coefficient, β_i and β_j are the linear terms, β_{ii} and β_{jj} are the quadratic terms and β_{ij} are the interaction parameter terms. P value with 95% confidence level was considered to evaluate the effectiveness of the model terms.

Preliminary design of experiment

In the first stage, an L_8 (2^7) orthogonal array (8 experiments) with seven degrees of freedom (DOF) was designed for investigation of the effects of seven factors including wire diameter, feed rate, voltage, carrier gas pressure, pulse time, fan pressure, and electrode distance (Table S1). The particle size of AlNPs were selected as the numerical response. XRD patterns give only crystallite size and not particle size but in monophase crystalline materials such as our AlNPs, the crystallite size is a good estimation of particle size. In addition, the XRD technique offers further valuable information about the purity of the AlNPs and possible formation of AlONPs. Therefore, the crystallite sizes determined from XRD patterns using the Scherer equation were selected as a measure of particle size of AlNPs (Table S2).[42]

Quantitatively, the contributions of carrier gas pressure and fan pressure were the least (0.37 and 0.014, respectively) and therefore, these factors were ignored for further studies.

The validity of the proposed model was proved by ANOVA (Table S3). The value of Prob > F for the model was less than 0.05 indicating the model is significant. The R^2-value 0.9962 implied that 99.62% of the variability in the data can be explained by the model. The predicted R-Squared of 0.9392 was in reasonable agreement with the Adjusted R-Squared of 0.9867. Adequate precision which measures the signal to noise ratio was 27.307 indicates an adequate signal.

The half-normal probability plot is a graphical tool that uses the relative contribution of all factors to determine which one is important or unimportant.[43,44] All factors close to the line should be considered while those coincide on the line have negligible effect on the response. In our study, all factors except carrier gas pressure and fan pressure had significant influence on the particle size of AlNPs (Figure 1).

The normality of data was checked by plotting a normal probability plot of the residuals. If the data points on the plot fall fairly close to the straight line, then the data are normally distributed.[45] The normal probability plot of the AlNPs showed such proximity to the straight line and indicated a normally distributed population (Figure 2). In addition, the plots of the residuals revealed that they have no obvious pattern and unusual structure. They also showed equal scatter above and below the x-axis. This implied that the model proposed is adequate and there is no reason to suspect any violation.[41]

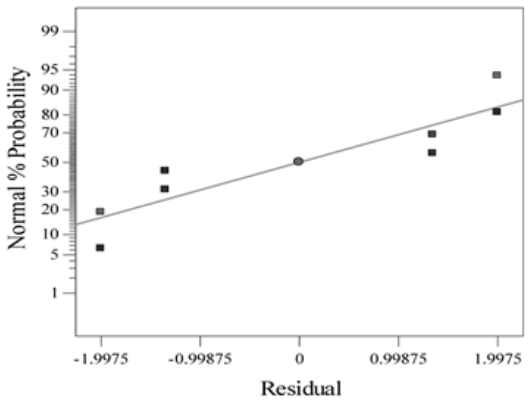

Figure 2. *Normal probability plot of residual for AlNPs for each factor based on preliminary design by Taguchi method.*

Final design of Experiments

In the last stage the remained five variables, wire diameter, feed rate, electrode distance, pulse time, and voltage, were studied comprehensively by Box Behnken response surface design method. The levels of the factors in coded and actual units are given in Table S4. Again, the particle size was selected as the numerical response. The experimental conditions and results obtained were shown in Table S5.

ANOVA results were presented in Table S6. The Model F-value of 104.26 implied the model was significant. There was only a 0.01% chance that such a large "Model F-Value" could occur due to noise. Values of Prob > F less than 0.0500 indicated all A, B, C, D, E terms were significant.

The Lack of Fit F-value of 9.35 implied the Lack of Fit was not significant relative to the pure error. The Predicted R-Squared of 0.9324 was in reasonable agreement with the Adjusted R-Squared of 0.9468. Adequate precision was 39.455 indicated an adequate signal. The validity of the final model was also evaluated using residual graphs (Figure 3).

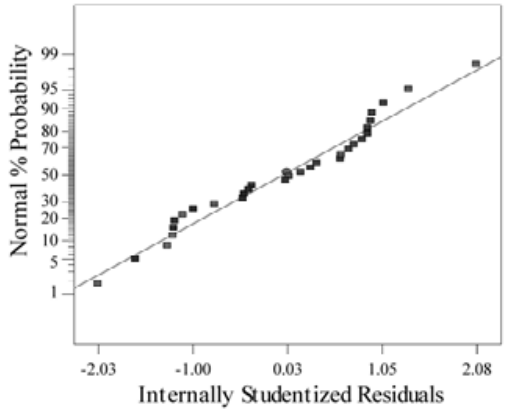

Figure 3. *Normal plot of residual based on final design by response surface method.*

The major factor determining the particle size in the EEW is superheating of the evaporated material i.e. $K = \frac{W}{W_s}$, where W is the energy injected into the evaporating wire and W_s is the sublimation energy of the wire, which diminishes when the diameter of the wire is reduced:

$$D = 0.3 \times 10^3 (W/W_s)^{-3} \quad (3)$$

For a typical experiment (Run 7), the predicted particle size based on the superheating was 27 nm which is in good agreement with the experimental result.

The modified coded equation (4) indicated the contribution of main factors on the particle size.

$$\text{particle size} = +106.51 + 9.63A + 15.19B + 18.40C + 13.85D - 30.64E \quad (4)$$

The results revealed that the order of contribution of factors in the particle size followed from the following trend:

Voltage > Electrode distance > Feed rate > Pulse time > Wire diameter.

In addition, apart from the voltage all factors show straight relationship with the particle size. The particle size increases with increasing all factor but the voltage (Figure 4). This inverse relationship between voltage and particle size is in agreement with previously reports[29] and is due to increase in the energy deposited in the wire during the increasing the voltage (5).

$$W_0 = \frac{1}{2} CV^2 \quad (5)$$

In where C, V and W_0 are capacity, voltage and the energy stored in the capacitor, respectively.[46,47]

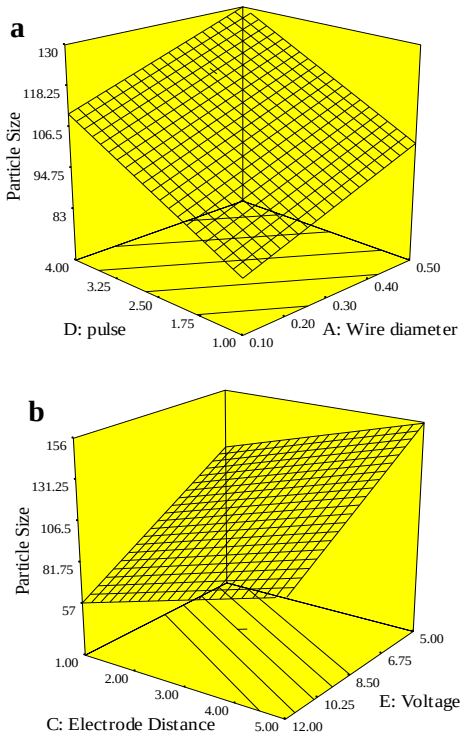

Figure 4. *Response surface plots for particle size: (a) Effects of wire diameter and pulse time on the response Actual factors (B= 2.5, C=3.0, E=8.5), (b) electrode distance and voltage on the response Actual factors (A=0.3, B=2.5, D=2.5).*

Correlation coefficient factor for electrode distance was 0.184 that meant this factor was the second effective factor on particle size. This effect is quite clear since overheat is inversely proportional to electrode distance and the particle size increase with decreasing the K values.

Correlation coefficient factor for feeding rate was 0.152 which placed it in the third place. Increasing the feeding rate resulted in decreasing the electrode distance as well as increasing the plasma volume in the chamber.[7,31]

An argon inert atmosphere with specified purge pulse was applied for gathering and conducting solid aerosols. Particle size increased with increasing pulse interval. Correlation coefficient factor for pulse time was 0.138.

Correlation coefficient factor for wire diameter was 0.096 which place it in the last place. Despite of unexpected least importance of wire diameter, it is clear that with increasing wire diameter, the superheating, K decreases and the particle size increases. This result was compatible with the results obtained previously.[47,48]

Process optimization

Process optimization depends on the target and herein was designed in order to obtain particles with size range 25 ± 5 nm. There were ten desired solutions for such target and the highlighted area on the overlay plot in Figure 5 shows one of them. In all solutions, the minimum required voltage was 11.40 kV and the maximum amount of required wire diameter was 0.20 mm.

An independent experiment (A, B, C, D, and E = 0.1, 4, 5, 2, and 8.5, respectively) was carried out to point prediction and verify the model. The particle size measured with XRD was 99.71 nm which is in agreement with the value 91.34 nm predicted.

In order to investigate the mass production potential of EEW, the experimental run 20 was done for 1 hour. The nanoparticles were collected and weighted. The yield was 60%.

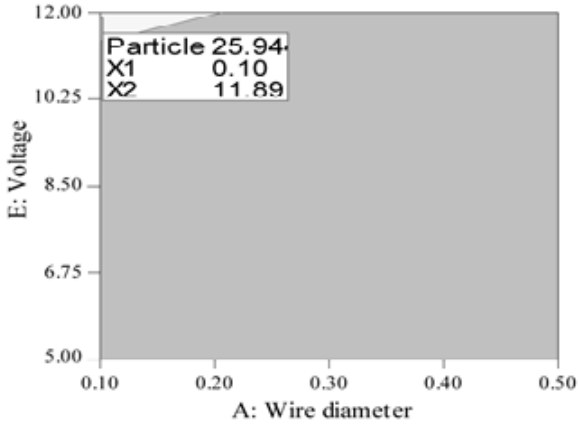

Figure 5. *Typically overlay plot for the optimal regions using response surface*

Characterization

AlNPs analyses

Typical TEM image of AlNPs is shown in Figure 6 (Experiment 7, Run 7). Particle size distributions based on the graphical image analysis of TEM are also given in Figure 6. The AlNPs were close to spherical in shape. Average particle size was 25.15 nm and particle distribution was in the range of 10-50 nm. The highest probability corresponded to 15-20 nm particles. Almost 88% of AlNPs had a size between 15-40 nm.

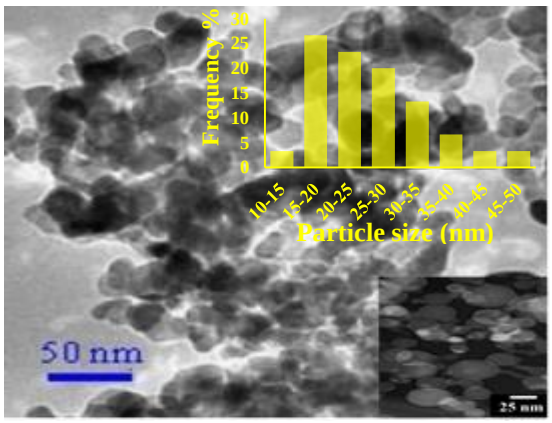

Figure 6. *Size distribution and morphology of AlNPs. Inset shows the size distribution of AlNPs obtained from TEM.*

A typical X-ray diffraction pattern of the prepared nanoparticles was shown in Figure 7 (Experiment 7, Run 7). The major patterns located at 2θ values 38.4°, 44.5°, 66.5°, and 78.1° were corresponded to (111), (200), (220), and (311) planes of AlNPs in a face-centered cubic structure as the main phase. (JCPDS 89-4034, a = b= c = 4.0494 Å) respectively. Additional weak patterns (35.1°, 44.5°, 57.0°, 37.4°, 45.5°, and 67.8°) were assigned for alumina as minor impurity due to probable oxidation of AlNPs surface. Repeating the procedure using argon atmosphere resulted in pure AlNPs.

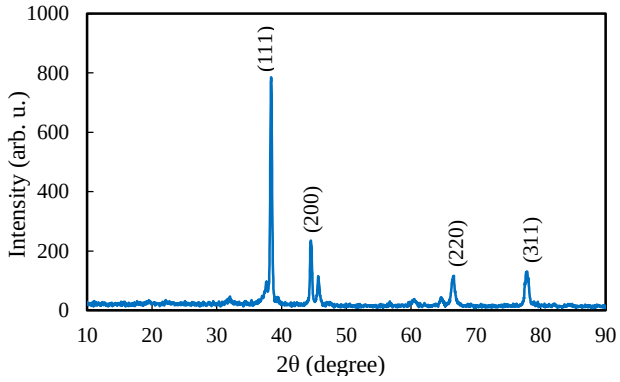

Figure 7. *Typically XRD patterns of AlNPs produced by EEW.*

The average particle size calculated from Debye-Scherer equation was 27.73 nm.[49] The result is in agreement with the value obtained by dynamic light scattering analysis shown in Figure 8. A very sharp peak for AlNPs at 28.21 nm with 100% intensity is observed (PDI = 0.384) which indicates a narrow distribution of nanoparticles of size 28.0 ± 5 nm.

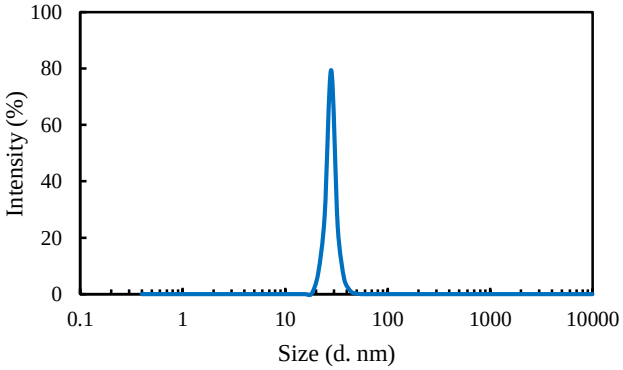

Figure 8. *Particle size distribution of AlNPs prepared by EEW method.*

AlONPs Analyses

AlONPs was produced easily in the oxygen atmosphere. A typical X-ray diffraction pattern of the prepared AlONPs was shown in Figure 9. The major patterns located at 2θ = 35.1°, 44.5°, and 57.0° are corresponded to (104), (400), and (116) planes of α- Alumina (JCPDS 46-1215) and 2θ values and 2θ values 37.4°, 45.5°, and 67.8° were three distinct reflections corresponded to (110), (400), and (440) planes of γ- Alumina (JCPDS 10-0425). Calculations of crystallite size using Debye-Scherer's equation showed that the α- and γ-phases of Al_2O_3 had an average crystallite size of about 9.0 nm and 26.0 nm, respectively.

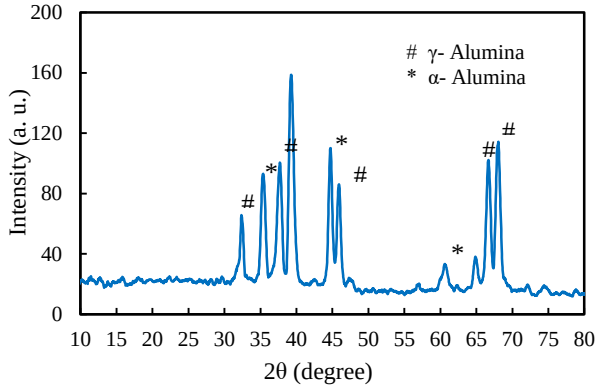

Figure 9. *XRD patterns of AlONPs produced by EEW.*

In the FT-IR spectrum of Al_2O_3 (Figure 10), a broad band centered at 3445 cm^{-1} was assigned to OH stretching of the adsorbed water or surface OH groups. The band at 1421 cm^{-1} is due to bending of molecular water.[50] Sharp peaks between 1000 and 500 cm^{-1} could be assigned to Al-O stretching.

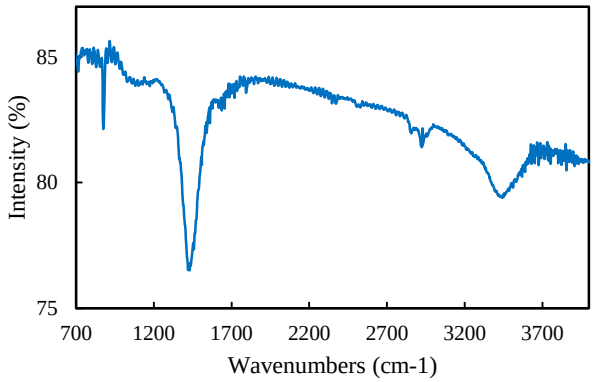

Figure 10. *FT-IR spectrum of synthesized AlONPs by EEW method.*

Dynamic light scattering showed a very sharp peak for AlONPs at 50.75 nm with 100% (PDI = 0.331) which indicates a narrow distribution of particle size 50.0 ± 5 nm (Figure 11).

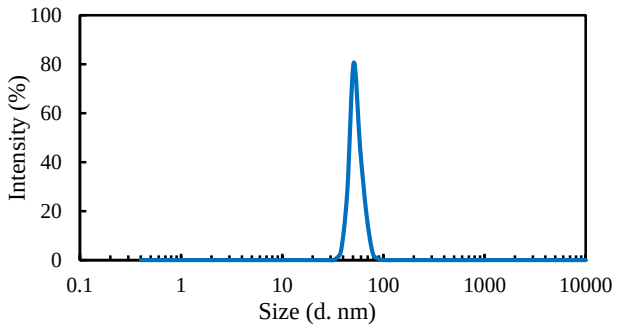

Figure 11. *Particle size distribution of AlONPs prepared by EEW method.*

Conclusions

In this work aluminum/alumina nanoparticles were produced in large scale by EEW process. This method is ecologically safe, useful for mass production, requires a relatively small energy, and allows making powders with a small degree of contamination. The EEW production of powders is of special interest since a considerable overheat of the metal and the nonequilibrium process allows for the preparation of the nanoparticles with such new properties as well controlled close to spherical and those which are expensive or difficult to produce by other methods. Analysis of variance was carried out to find main effect factors and optimization of conditions for synthesizing nanoparticles. It is found that the voltage, electrode distance, feed rate, pulse time, and wire diameter were the most effective factors. The particle size increases when the voltage decreases and decreases when other factors increase. The values of model adequacy indicators show a good correlation between experimental data and those obtained based on mathematical equations of models developed.

References

1. Y. Lee, J. Choi, K. J. Lee, N. E. Stott, D. Kim, *Nanotechnology*, 19, **2008**, 415604.
2. R. Baetens, B. Petter Jelle, A. Gustavsen, *Sol. Energy Mater. Sol. Cells*, 94, **2010**, 87.
3. L. Gao, Q. Zhang, *Scr. Mater.*, 44, **2001**, 1195.
4. T. d. F. Silva, J. A. C. Dias, C. G. Maciel, J. M. Assaf, *Catal. Sci. Technol.,* 3, **2013**, 635.
5. Y. A. Kotov, E. A. Litvinov, S. Y. Sokovinin, M. E. Balezin, V. R. Khrustov, *Dokl. Phys.*, 45, **2000**, 18.
6. D. A. Kaplowitz, G. Jian, K. Gaskell, A. Ponce, P. Shang, M. R. Zachariah, *Part. Part. Systems Character.,* 30, **2013**, 881.
7. Y. S. Lee, B. Bora, S. L. Yap, C. S. Wong, *Curr. Appl. Phys.*, 12, **2012**, 199.
8. A. Rai, K. Park, L. Zhou, M. R. Zachariah, *Combust. Theor. Model.*, 10, **2006**, 843.
9. K. Park, D. Lee, A. Rai, D. Mukherjee, M. R. Zachariah, *J. Phys. Chem. B*, 109, **2005**, 7290.
10. B. C. Gates, *Chem. Rev.*, 95, **1995**, 511.
11. A. Krell, H. W. Ma, *J. Am. Ceram. Soc.*, 86, **2003**, 241.
12. G. Dimas-Rivera, J. de la Rosa, C. Lucio-Ortiz, J. De los Reyes Heredia, V. González, T. Hernández, *Materials*, 7, **2014**, 527.
13. M. Mende, I. Balasa, H. Ehlers, D. Ristau, D. B. Douti, L. Gallais, M. Commandré, *Appl. Optics*, 53, **2014**, A383.
14. Y. S. Kwon, A. A. Gromov, J. I. Strokova, *Appl. Surf. Sci.*, 253, **2007**, 5558.
15. M. Kakati, B. Bora, U. P. Deshpande, D. M. Phase, V. Sathe, N. P. Lalla, T. Shripathi, S. Sarma, N. K. Joshi, A. K. Das, *Thin Solid Films*, 518, **2009**, 84.
16. M. Gazanfari, M Karimzadeh, S. Ghorbani, M. R. Sadeghi, G. Azizi, H. Karimi, N. Fattahi, Z. Karimzadeh, *Bull. Mater. Sci.*, 37, **2014**, 871.
17. S. Ghanta, K. Muralidharan, *J. Nanopart. Res*, 15, **2013**, 1715.
18. S. Al mamun, R. Nakajima, T. Ishigaki, *J Colloid Interface Sci.*, 392, **2012**, 172.
19. N. Arora, B. R. Jagirdar, *J. Mater. Chem.,* 22, **2012**, 9058.
20. R. G. Palgrave, I. P. Parkin, *New J. Chem.*, 30, **2006**, 505.
21. Yu. A. Kotov, *J. Nanopart. Res.*, 5, **2003**, 539.
22. R. Sarathi, T. K. Sindhu, S. R. Chakravarthy, *Mater. Charact.*, 58, **2007**, 148.
23. R. Sarathi, T. K. Sindhu, S. R. Chakravarthy, *Mater. Lett.*, 61, **2007**, 1823.

24. Y. Tokoi, T. Suzuki, T. Nakayama, H. Suematsu, F. Kaneko, K. Niihara, *Curr. Appl. Phys.*, 9, **2009**, S193.
25. L. Liu, J. Zhao, W. Yan, Q. Zhang, *IEEE T. Nanotechnol.*, 13, **2014**, 842.
26. S. H. Tong, Z. X. Bing, Z. Shen, Z. X. Lei, W. X. Xin, *Acta Phys. Sin*., 63, **2014**, 145206.
27. V. S. Sedoi, Y. F. Ivanov, 19, **2008**, 145710.
28. I. V. Beketov, A. P. Safronov, A. I. Medvedev, J. Alonso, G. V. Kurlyandskaya, S. M. Bhagat, *AIP Advances*, 2, **2012**, 022154.
29. Q. Li, Q. Z. Song, J. Z. Wang, Y. X. Duo, *Surf. Coat. Tech.*, 206, **2011**, 202.
30. S. Aravinth, B. Sankar, S. R. Chakravarthi, R. Sarathi, *Mater. Charact.*, 62, **2011**, 248.
31. R. Sarathi, T. K. Sindhu, S. R. Chakravarthy, A. Sharma, K. V. Nagesh, *J. Alloy. Compd.*, 475, **2009**, 658.
32. M. Barmala, A. Mohe, R. Emadi, *J. Alloy. Compd.*, 485, **2009**, 778.
33. C. J. Tighe, R. Q. Cabrera, R. I. Gruar, J. A. Darr, *Ind. Eng. Chem. Res.*, 52, **2013**, 5522.
34. S. Vorob'ev , S. P. Malyshenko, S. I. Tkachenko, *High Temp.*, 43, **2005**, 908.
35. Q. Zhou, Q. Zhang, W. Yun, X. Liu, J. Zhang, J. Zhao, L. Pang, *IEEE Transactions on Plasma Sci.*, 40, **2012**, 2198.
36. K. Jayaraman, S. R. Chakravarthy, R. Sarathi, *Proc. Combust. Inst.*, 33, **2011**, 1941.
37. R. Abedini, S. M. Mousavi, *Chem. Ind. Chem. Eng.* Q., 18, **2012**, 171.
38. K. K. Tan, K. Z. Tang, *Eur. J. Oper. Res.*, 128, **2001**, 545.
39. T. Y. Lin, C. H. Tseng, *Eng. App. Artif. Intel.*, 13, **2000**, 3.
40. R. X. K. Gao, W. J. R. Haefer, L. R-Ping, *IEEE T. Anten. Propag*, 62, **2014**, 2102.
41. M. Darvishpour, M. Feyzi, M. Joshaghani, *Bulgharian Chem. Commun.*, 48, **2016**, 156.
42. E. J. Park, S. W. Lee, I. C. Bang, H. W. Park, *Nanoscale Res. Lett.*, 6, **2011**, 223.
43. L. C. Chang, S. C. Wu, J. W. Tsai, T. J. Yu, T. R. Tsai, *Int. J. Pharm.*, 376, **2009**, 195.
44. B. Rahmanian, M. Pakizeh, S. A. A. Mansoori, R. Abedini, *J. Hazard. Mater.*, 187, **2011**, 67.
45. K. Muzyka, K. Karim , A. Guerreiro, A. Poma, S. Piletsky, *Nanoscale Res. Let.*, A 9, **2014**, 154.
46. Y. S. Kwon, Y. H. Jung, N. A. Yavorovsky, A. P. Illyn and J. S. Kim, *Scripta mater*., 44, **2001**, 2247.
47. P. Wankhede, P. K. Sharma, A. K. Jha, *J. Eng. Res. Appl*., 3, **2013**, 1664.
48. O. Giuca, I. Grozescu, *Chem. Bull*., 56, **2011**, 105.
49. A. L. Ortiz, L. Shaw, *Acta Mater*., 52, **2004**, 2185.
50. T. M. H. Costa, M. R. Gallas, E. V. Benvenutti, J. A. H. da Jornada, *J. Phys. Chem. B*, 103, **1999**, 4278.